PHYSICAL REVIEW MATERIALS **1**, 075408 (2017)

Real-space study of the optical absorption in alternative phases of silicon

Chin Shen Ong,[1] Sinisa Coh,[1,2] Marvin L. Cohen,[1] and Steven G. Louie[1,*]

[1]*Department of Physics, University of California at Berkeley and Materials Sciences Division, Lawrence Berkeley National Laboratory, Berkeley, California 94720, USA*

[2]*Materials Science and Engineering, Mechanical Engineering, University of California Riverside, Riverside, California 92521, USA*

(Received 29 June 2017; published 27 December 2017)

We introduce a real-space approach to understand the relationship between optical absorption and crystal structure. We apply this approach to alternative phases of silicon, with a focus on the Si_{20} crystal phase as a case study. We find that about 83% of the changes in the calculated low-energy absorption in Si_{20} as compared to Si in the diamond structure can be attributed to reducing the differences between the on-site energies of the bonding and antibonding orbitals as well as increasing the hopping integrals for specific Si-Si bonds.

DOI: 10.1103/PhysRevMaterials.1.075408

I. INTRODUCTION

In order to reduce the cost of solar-cell energy generation, a great deal of effort has been put into attempts to increase the number of charge carriers collected by the solar cell relative to the number of incident photons (quantum efficiency). Silicon is the most widely used photovoltaic material. In terms of global annual power production, a recent market survey shows that crystalline silicon dominates the photovoltaic industry by more than 90%. One of the major reasons for its popularity is that silicon is nontoxic and abundant. There are also benefits from technologies developed over the years in the microelectronics industry.

Despite its widespread usage as a photovoltaic material, silicon does not efficiently absorb most of the light in the solar spectrum. The solar spectrum that is received at the Earth's surface (under the so-called air mass of 1.5 or AM 1.5 for short [1]) ranges from 0.3 to 4.4 eV and is the strongest around 1.2 eV. According to the Shockley-Quiesser model [2], the optimal band gap for solar energy conversion lies within the range of 1.1 to 1.4 eV [2–4]. Since silicon has a direct band gap of 3.3 eV, optical absorption due to direct transitions can only take place at the high-energy end of the solar spectrum between 3.3 and 4.4 eV. Phonon-assisted indirect transitions lower the onset of optical absorption to about 1.0–1.2 eV [5,6]. Even then, absorption coefficients due to indirect transitions alone are smaller and the solar cell has to be thick in order to amplify the phonon contributions. With a thicker absorber layer, the solar cell has to have high purity to prolong its carriers lifetime. Together, the increased thickness and need for material purity add to the cost of production.

Under ambient conditions, the diamond-cubic phase (diamond-Si) is the most stable crystal phase of silicon, and this is also the crystal phase of silicon most commonly used to make solar cells today. However, silicon is known to exist in other crystal phases as well. For instance, with increase in pressure, silicon undergoes phase transitions from the diamond-Si phase to the β-Sn phase [7], *Imma* phase [8], simple hexagonal phase [9–12], and *Cmca* phase [13]. Pressure release from the β-Sn phase does not recover the diamond-Si phase. Instead, a slow pressure release produces the metastable R8 phase [14] which subsequently transforms into the BC8 phase [15–18], while a very rapid pressure release leads to two other tetragonal phases [19]. Many of these phases are not suitable to make solar cells. For example, the first four phases mentioned above only exist under high pressure. The β-Sn and simple hexagonal phases are also metallic [11,12], while the BC8 phase [18] is semimetallic. On the other hand, phases like the R8 [20] and body-centered tetragonal [21] phases are semiconducting, and since they have direct band gaps smaller than diamond-Si's, they in principle can also absorb light over a wider energy range [22] than diamond-Si. Recently, a low-density silicon allotrope with an open silicon framework consisting of large empty channels, Si_{24}, has reportedly [23] been synthesized. It has a direct G_0W_0 band gap of 1.34 eV, which is smaller than that of diamond-Si.

One approach [22] to increasing the absorption range of silicon is then to find a crystal phase of silicon that has a smaller direct band gap than that of diamond-Si. With the advent of first-principles computational techniques, it has become possible to search [24–27] for crystal phases that have not been previously discovered. Botti *et al.* [28] found several crystal phases of silicon that have lower energies than the R8 and BC8 phases and have quasiparticle band gaps ranging from 0.8 to 1.5 eV from GW calculations. Wang *et al.* [29] proposed phases of silicon that have band gaps from 0.39 to 1.25 eV obtained within density functional theory (DFT) using the hybrid HSE functional. Lee *et al.* [30] used the conformational space annealing (CSA) approach and presented several other direct-gap silicon phases. Using the same CSA approach, Oh *et al.* [31] subsequently proposed a series of direct-gap silicon superlattices composed of bulklike Si layers intercalated by defective layers made of Seiwatz chains [32]. Depending on the thicknesses of the bulklike layers, these superlattices can have calculated G_0W_0 band gaps that fall within the optimal energy range for solar conversion, according to the Shockley-Quiesser model [2–4].

In Ref. [33], Xiang *et al.* found the structure of Si_{20} (also called Si_{20}-T) using the particle swarm optimization (PSO) [24] approach. The calculated DFT-HSE band gap of Si_{20} is 1.55 eV. One of the structural features of Si_{20}, which is not found in diamond-Si, is that some of the bonds form equilateral triangles. In Ref. [33], it was suggested that these bonds may be related to the improved optical absorption of Si_{20} in the low-energy regime. Nevertheless, the microscopic reason for the increase in the calculated absorption in Si_{20} remains unknown. In another work, Guo *et al.* [34] proposed an alternative ground

---

[*] sglouie@berkeley.edu

state of silicon that also contains triangular bonds and has a calculated DFT-HSE band gap of 0.61 eV.

The purpose of this work is to understand how the structure of an alternative silicon phase may lead to an improved calculated optical absorption for photovoltaic applications relative to diamond-Si. While there are many proposed metastable phases of silicon with improved absorption, we focus here in detail on Si_{20} as a case study for our approach since it has a very desirable calculated optical absorption spectrum. (We note that Si_{20} has a somewhat high formation energy [30,35,36], which may make it harder to access experimentally.) To demonstrate the generality of our approach, near the end of this paper, we also study two other silicon phases (SC5 and Si_{24}) that have drastically different structures from that of Si_{20}.

One of the obstacles in establishing the relationship between the crystal structure and optical absorption is the fact that the crystal structures of alternative phases of silicon like Si_{20} and diamond-Si are very different. For example, one cannot be related to the other by the removal or addition of a single atom, or by a small structural distortion that will not drastically disturb the bonding network of the silicon atoms. Moreover, the primitive unit cell of diamond-Si contains two atoms, whereas that of Si_{20} contains 20 atoms. Therefore, a conventional analysis of optical absorption in the reciprocal space is nontrivial as each k point in Si_{20} contains 40 valence and 40 conduction sp^3-like bands, unlike diamond-Si, which only has four of each.

To overcome this difficulty, we study the optical absorption in a real-space representation using Wannier functions. Our analysis reveals that about 33% of the enhanced optical absorption of Si_{20} can be attributed to the decreased differences of the on-site energies between the bonding and antibonding orbitals. Roughly 50% is due to the increased hopping integrals between the bonding and antibonding orbitals. The remaining 17% is due to a variety of other contributions.

II. METHOD

In this section we will first describe the conventional density functional theory (DFT) interband-transition approach and the GW plus Bethe-Salpeter equation (GW-BSE) approach for computing optical absorption in reciprocal space. The latter approach includes electron self-energy and electron-hole (excitonic) effects. Next, we briefly introduce a real-space representation of the electronic structure in terms of Wannier functions. Finally, we transform the expression for the optical absorption from the reciprocal-space representation into the real-space representation.

A. Optical absorption

Optical absorption can be expressed through $\epsilon_2(\omega)$, the imaginary part of the dielectric function. Within the independent-particle DFT approach and neglecting the photon momentum, the diagonal elements of $\epsilon_2(\omega)$ can be computed using the random-phase approximation (RPA) for a specific light polarization,

$$\epsilon_2(\omega) = 8\pi^2 e^2 \hbar^2 \sum_{\mathbf{k}} \sum_{n\in\{C\}} \sum_{m\in\{V\}} |\mathbf{e}\cdot\langle n\mathbf{k}|\mathbf{r}|m\mathbf{k}\rangle|^2 \times \delta(\hbar\omega - E_{n\mathbf{k}} + E_{m\mathbf{k}}). \quad (1)$$

Here $\mathbf{k}$ is the wave vector, $\mathbf{e}$ is the polarization direction, $\mathbf{r}$ is the position operator, ω is the frequency of absorbed photon, $E_{n\mathbf{k}}$ and $E_{m\mathbf{k}}$ are the DFT eigenvalues, $|n\mathbf{k}\rangle$ and $|m\mathbf{k}\rangle$ are the DFT Bloch eigenstates, and $\{V\}$ and $\{C\}$ are the valence and conduction bands. The matrix element $\langle n\mathbf{k}|\mathbf{r}|m\mathbf{k}\rangle$ describes a transition of an electron from state $|m\mathbf{k}\rangle$ into state $|n\mathbf{k}\rangle$ upon the absorption of a photon.

(a) DFT-RPA absorption

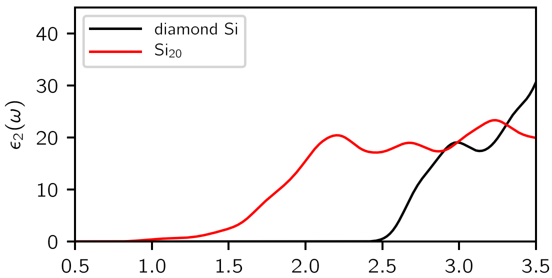

(b) GW-BSE absorption

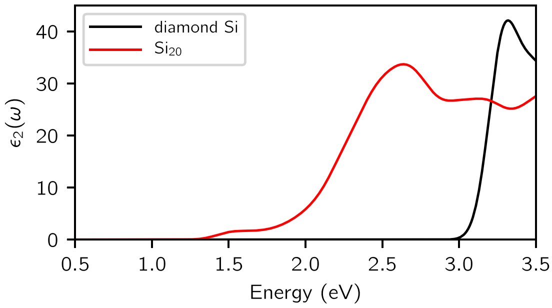

FIG. 1. Optical absorption spectra of diamond-Si (black) and Si_{20} (red) calculated using the DFT-RPA (a) and GW-BSE (b) approaches.

The $\epsilon_2(\omega)$ calculated within the DFT-RPA approach is shown in Fig. 1(a) for diamond-Si (black) and Si_{20} (red). In this calculation, we use a norm-conserving pseudopotential and the local density approximation as implemented in Quantum-ESPRESSO [37]. The plane-wave cutoff for the electron wave function is 36 Ry. For diamond-Si, the Wannier functions are constructed from a coarse k mesh of 16×16×16 and they are used to interpolate quantities on a fine k mesh of 30×30×30 to calculate $\epsilon_2(\omega)$. For Si_{20}, the coarse k mesh is 8×8×8 and the fine k mesh is 20×20×20.

From Fig. 1(a), it is clear that within the DFT-RPA approach, the onset of optical absorption in Si_{20} is 1.7 eV lower in energy than that in diamond-Si. However, optical absorption in Si_{20} at the absorption edge is relatively small, and it increases significantly only at 0.8 eV above the absorption edge. Comparing the steep edges of the absorption spectra, the steep edge of Si_{20} is still about 0.9 eV lower in energy than it is for diamond-Si.

In what follows, we discuss two well-known limitations of the optical absorption calculated within the DFT-RPA approach. The first limitation is that the calculated DFT-LDA band gap is typically too small due the fact that DFT eigenvalues are not quasiparticle excitation energies. The GW approximation [38] removes this limitation by properly including the electron self-energy effects. In the case of Si_{20} and diamond-Si, the inclusion of the GW correction [39] separates the DFT valence and conduction bands by 0.7–0.8 eV (depending on the k points and electron bands) which is close to the value obtained by the hybrid-functional approach used in Ref. [33].

The second limitation of the optical absorption calculated within the DFT-RPA approach is that it does not consider electron-hole interactions. Within the interacting many-electron picture, an electron is excited from a ground state $|0\rangle$ to an excited excitonic state $|S\rangle$, in which the electron interacts with the hole that it has left behind. This process can be calculated [40] by solving the BSE and $\epsilon_2(\omega)$ is then expressed as

$$\epsilon_2(\omega) = 8\pi^2 e^2 \hbar^2 \sum_S |\mathbf{e}\cdot\langle S|\mathbf{r}|0\rangle|^2 \delta(\hbar\omega - \Omega_S). \tag{2}$$

Here S labels the exciton states and Ω_S is the exciton eigenenergy.

The $\epsilon_2(\omega)$ spectra calculated [39] by solving the BSE for Si_{20} and diamond-Si are shown in Fig. 1(b). Comparing the GW-BSE and DFT-RPA absorption spectra, we see two main differences. First, the absorption edge in the GW-BSE spectrum is 0.6 eV higher in energy than the edge in the DFT-RPA spectrum. This shift is close to the shift resulting from the GW correction (0.7 eV). The second difference with the GW-BSE approach is that $\epsilon_2(\omega)$ is larger in amplitude by a factor of about 1.5–2.0 near the band edge.

Therefore, while the optical absorption in absolute terms is very different between the GW-BSE and DFT-RPA approaches, the corrections made by the GW-BSE approach are nearly the same for both Si_{20} and diamond-Si. To better understand the improved absorption of Si_{20}, it is sufficient to focus on an analysis of results from the DFT-RPA approach, since the geometric effect of the crystal structure is already present at the DFT-RPA level.

B. Localized representation

The Bloch states appearing in the expression for $\epsilon_2(\omega)$ [in Eq. (1)] have a well-defined crystal momentum $\mathbf{k}$. They are eigenstates of the Kohn-Sham Hamiltonian,

$$\langle n\mathbf{k}|H|m\mathbf{k}\rangle = \delta_{nm} E_{n\mathbf{k}}. \tag{3}$$

By superposing the Bloch states of different crystal momenta $\mathbf{k}$, one can construct a well localized Wannier state,

$$|j\mathbf{R}\rangle = \frac{1}{N_\mathbf{k}} \sum_{n\mathbf{k}} e^{-i\mathbf{k}\cdot\mathbf{R}} U_{nj}^{(\mathbf{k})} |n\mathbf{k}\rangle . \tag{4}$$

Here $\mathbf{R}$ is a real-space lattice vector and $U_{nj}^{(\mathbf{k})}$ is an arbitrary unitary matrix that mixes the Bloch bands at $\mathbf{k}$. In this paper, we use indices i and j to denote individual Wannier functions and indices n and m to denote individual Bloch bands.

One often chooses the matrices $U_{nj}^{(\mathbf{k})}$ according to the scheme introduced by Marzari and Vanderbilt [41] so that $|j\mathbf{R}\rangle$ is as localized in real space around the centers of mass of the Wannier functions as possible. For this reason, $|j\mathbf{R}\rangle$ is also called the maximally localized Wannier function. The Bloch functions can be reconstructed back from the Wannier functions through an inverse transformation,

$$|n\mathbf{k}\rangle = \sum_{j\mathbf{R}} e^{i\mathbf{k}\cdot\mathbf{R}} U_{nj}^{(\mathbf{k})\dagger} |j\mathbf{R}\rangle . \tag{5}$$

(a) Bonding Wannier function

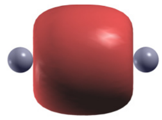

(b) Antibonding Wannier function

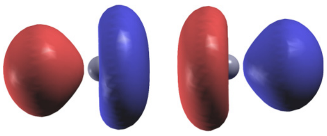

FIG. 2. Isosurfaces of the calculated bonding (a) and antibonding (b) Wannier functions in diamond-Si. Gray spheres represent the silicon atoms forming the bond. Isosurface in (a) is 1.4 and 1.0 in (b). Red and blue colors indicate parts of the Wannier function with opposite signs.

Since the set of Wannier functions contains the same amount of information as the set of Bloch bands from which it is generated, it is convenient to rewrite the Hamiltonian and position operators in the Wannier basis. The Hamiltonian in the Wannier (or real-space) representation is simply $\langle i\mathbf{0}|H|j\mathbf{R}\rangle$ which can be calculated by a Fourier transform of $\langle n\mathbf{k}|H|m\mathbf{k}\rangle$,

$$\langle i\mathbf{0}|H|j\mathbf{R}\rangle = \frac{1}{N_\mathbf{k}} \sum_{nm\mathbf{k}} e^{-i\mathbf{k}\cdot\mathbf{R}} U_{ni}^{(\mathbf{k})\dagger} \langle n\mathbf{k}|H|m\mathbf{k}\rangle\, U_{mj}^{(\mathbf{k})}. \tag{6}$$

There are two types of Hamiltonian matrix elements that we will focus on in this paper. For the first type, we have $\mathbf{R} = \mathbf{0}$ and $i = j$. We will refer to this type of matrix elements

$$\langle i\mathbf{0}|H|i\mathbf{0}\rangle = e_{i,} \tag{7}$$

as the on-site energy of Wannier function i. The remaining matrix elements

$$\langle i\mathbf{0}|H|j\mathbf{R}\rangle = t_{ij\mathbf{R}} \tag{8}$$

are known as the hopping integrals. The hopping integral represents the probability amplitude for Wannier function j in cell $\mathbf{R}$ to tunnel to the Wannier function i in the cell at the origin.

Wannier functions are constructed from a set of Bloch bands so a different choice of Bloch bands will lead to different Wannier functions. Since the expression for optical absorption in Eq. (1) refers explicitly to occupied and empty Bloch states, we constructed the Wannier functions either from only empty or only occupied Bloch states. As a result, by construction, $\langle i\mathbf{0}|H|j\mathbf{R}\rangle$ is zero unless the bra and ket are either both derived from empty or occupied states.

We will refer to the Wannier functions constructed from the occupied Bloch states as bonding Wannier functions and those from the empty states of the relevant conduction bands as antibonding Wannier functions since they typically have real-space forms that resemble bonding and antibonding molecular orbitals. As silicon bonds are highly covalent, the valence charges are localized on the bonds between these two nearest-neighboring silicon atoms. Therefore, the bonding and antibonding Wannier states are localized in the region between these two silicon atoms, as shown in Fig. 2 for diamond-Si. Each Si-Si bond has only one sp^3-like bonding

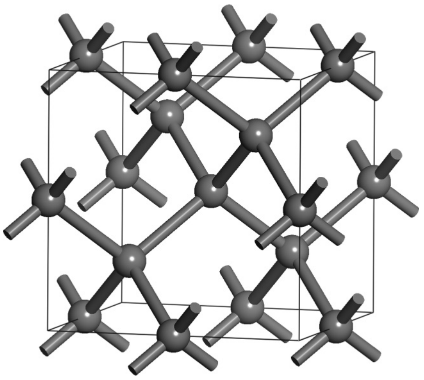

FIG. 3. Conventional unit cell of diamond-Si containing eight silicon atoms. Its primitive unit cell contains only two silicon atoms.

and one sp^3-like antibonding Wannier function (per spin). For convenience, we will label the on-site energy for the bonding and antibonding states as,

$$e_i \quad \text{and} \quad \bar{e}_i,$$

respectively. Similarly, we denote the hopping integral between antibonding states as $\bar{t}_{ij\mathbf{R}}$.

C. Optical absorption in the localized basis

The optical absorption spectrum calculated using $\epsilon_2(\omega)$ [Eq. (1)] within the DFT-RPA approach depends on the energy of the Bloch states $E_{n\mathbf{k}}$, and the matrix elements of the position operator. The Bloch state energies are fully determined by e_i and $t_{ij\mathbf{R}}$. Similarly, the position operator matrix element can be computed from its representation in the Wannier basis

$$\langle i\mathbf{0}|\mathbf{r}|j\mathbf{R}\rangle = \mathbf{r}_{ij\mathbf{R}}. \tag{9}$$

In all, optical absorption is exactly determined given these three real-space quantities: e_i, $t_{ij\mathbf{R}}$, and $\mathbf{r}_{ij\mathbf{R}}$.

III. RESULTS AND DISCUSSION

In this section, we will compare e_i, $t_{ij\mathbf{R}}$, and $\mathbf{r}_{ij\mathbf{R}}$ in diamond-Si and Si_{20} and relate them to the structural differences between the two materials, as well as the differences in their optical absorptions.

A. Comparison of structures

Figures 3 and 4 show the crystal structures of diamond-Si and Si_{20}. Both of their conventional unit cells have cubic lattices. In our calculations, we use fully-relaxed structures of Si_{20} and diamond-Si. The lattice parameters of the conventional unit cells of Si_{20} and diamond-Si are 7.40 and 5.43 Å. On the average, Si_{20} has one Si atom every 20.2 Å^3 (2.30 g/cm^3) and diamond-Si has one atom every 20.0 Å^3 (2.33 g/cm^3).

Each Si atom in diamond-Si is tetrahedrally coordinated to four other Si atoms, such that every bond angle is exactly 109.5°. Every Si-Si bond in diamond-Si is symmetrically equivalent. The distance between the bond centers of two nearest-neighboring bonds is 1.9 Å.

For Si_{20}, every Si atom is also coordinated to four other Si, but in a distorted tetrahedron. The distortions bring some of the bond centers of Si_{20} closer together and others further apart. There are four symmetry-inequivalent groups of Si-Si bonds in Si_{20} and they are labeled from a to d in Fig. 4. One feature of the Si_{20} structure is the type-a bonds which form triangles. These bonds are highly strained as they are distorted from 109.5° to a narrow 60.0°. As a result, the distance between two nearest-neighboring bond centers of Si_{20} ranges from as short as 1.2 Å (between two type-a bonds of the same triangle) to 2.1 Å. We will label this range, 1.2–2.1 Å, as the nearest-neighbor hopping regime.

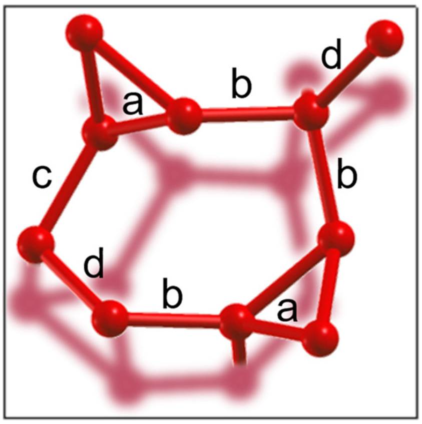

FIG. 4. Conventional unit cell of Si_{20} containing 20 silicon atoms. Its primitive unit cell is the same as its conventional unit cell. The four distinct Si-Si bonds are labeled using the letters a, b, c, and d. Bonds forming a triangle are labeled with the letter a.

B. On-site energy e_i

Here we compare on-site energies of diamond-Si and Si_{20}. Since we can assign a single bonding and antibonding Wannier function to each Si-Si bond, we will focus here on comparing the on-site energies, e_i and $\bar{e}_i$, for the same bond in the crystal.

Calculated values of e_i and $\bar{e}_i$ for diamond-Si and Si_{20} are shown in Fig. 5 with horizontal lines. The arrow represents the difference between e_i and $\bar{e}_i$ for a given set of symmetry-related bonds in the structure. In the case of diamond-Si, $\bar{e}_i - e_i$ for its Si-Si bonds is 9.66 eV. On the other hand, $\bar{e}_i - e_i$ for Si_{20}

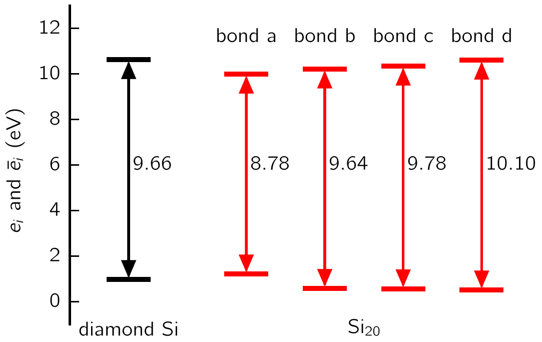

FIG. 5. On-site energy of bonding (e_i, lower value) and antibonding ($\bar{e}_i$, higher value) Wannier function in diamond-Si (left, black) and Si_{20} (right, red). Numbers indicate $\bar{e}_i - e_i$ in eV. In the case of Si_{20} we show $\bar{e}_i - e_i$ for all four types of bonds. (The origin of the energy scale is arbitrary.)

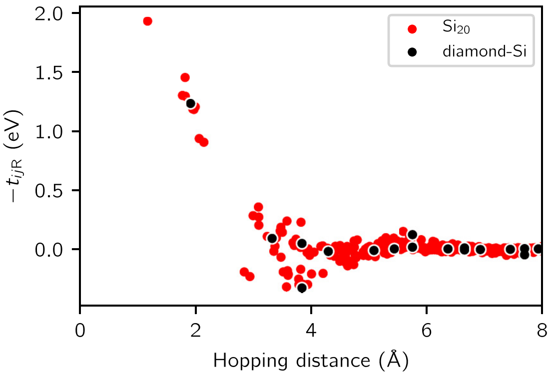

FIG. 6. Hopping integrals between bonding Wannier functions, as a function of hopping distance for diamond-Si (black) and Si$_{20}$ (red).

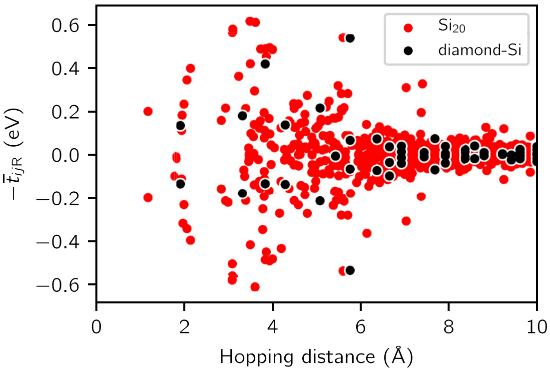

FIG. 7. Hopping integrals between antibonding Wannier functions, as a function of hopping distance for diamond-Si (black) and Si$_{20}$ (red).

ranges from 8.78 to 10.10 eV. The smallest value (8.78 eV) belongs to the highly-strained type-a bonds. Its large deviation from diamond-Si's 9.66 eV is likely due to the large strain present in these triangular bonds. Less strained type-b and type-c bonds have $\bar{e}_i - e_i$ (9.64 and 9.78 eV) similar to that in diamond-Si. Finally, type-d bonds have the largest $\bar{e}_i - e_i$ (10.10 eV).

We expect that the smaller $\bar{e}_i - e_i$ of type-a bonds will lower the optical absorption edge of Si$_{20}$ with respect to diamond-Si's. This will be analyzed in more detail in Sec. III E.

C. Hopping integral $t_{ij\mathbf{R}}$

After analyzing e_i, we now focus on the hopping integral $t_{ij\mathbf{R}}$ of diamond-Si and Si$_{20}$.

For the analysis of $t_{ij\mathbf{R}}$, we will define the hopping distance as the distance between the centers of mass of the Wannier functions $|i\mathbf{0}\rangle$ and $|j\mathbf{R}\rangle$,

$$\left| \langle i\mathbf{0}|\mathbf{r}|i\mathbf{0}\rangle - \langle j\mathbf{R}|\mathbf{r}|j\mathbf{R}\rangle \right|.$$

In what follows, we will relate $t_{ij\mathbf{R}}$ with its hopping distance.

1. Bonding states

First, we discuss the hopping integrals between bonding Wannier functions. As shown in Fig. 6, the hopping integrals of both diamond-Si and Si$_{20}$ are nearly zero for hopping distances beyond 5 Å. This behavior is characteristic of the exponential localization [42] of Wannier functions for insulators.

The hopping integral $t_{ij\mathbf{R}}$ with the largest magnitude for diamond-Si is −1.23 eV. This hopping integral couples a bonding Wannier function with its nearest-neighboring bonding Wannier functions and has a hopping distance of 1.9 Å. In Fig. 6, it is denoted by the leftmost black dot. For Si$_{20}$, hopping integrals coupling the nearest-neighboring bonding Wannier functions are distributed over the range of 1.2–2.1 Å (see Sec. III A). In Fig. 6, they are represented by the group of red dots surrounding the above-mentioned black dot.

The largest $|t_{ij\mathbf{R}}|$ for Si$_{20}$ corresponds to the hopping integral with the shortest hopping distance of 1.2 Å. This hopping integral couples type-a bonds and is 0.70 eV larger than the largest $|t_{ij\mathbf{R}}|$ of diamond-Si. The presence of this large hopping integral in Si$_{20}$ is due to the fact that the distance between triangular bonds is 1.9–1.2 = 0.7 Å shorter than the shortest bond–bond distance in diamond-Si.

As we will analyze in more detail in Sec. III E, we expect the larger hopping integrals of the occupied Wannier functions to raise the valence band edge of Si$_{20}$ since we expect the valence bands to have a larger bandwidth.

2. Antibonding states

Now we look at the hopping integrals between the antibonding states. Figure 7 shows that the largest $|\bar{t}_{ij\mathbf{R}}|$ for diamond-Si is 0.54 eV and has a hopping distance of 5.8 Å. Unlike the bonding states, this largest $\bar{t}_{ij\mathbf{R}}$ does not couple the nearest-neighboring Wannier functions. That hopping integral is four times smaller (0.13 eV). For Si$_{20}$, the largest $|\bar{t}_{ij\mathbf{R}}|$ is 0.62 eV and has a hopping distance of 3.5 Å. It is somewhat larger than diamond-Si's largest $|\bar{t}_{ij\mathbf{R}}|$ and it also does not couple the nearest-neighboring Wannier functions.

Nevertheless, in the nearest-neighbor hopping regime of 1.2–2.1 Å, the largest $|\bar{t}_{ij\mathbf{R}}|$ of Si$_{20}$ is 0.40 eV. This value is significantly larger than the corresponding $|\bar{t}_{ij\mathbf{R}}|$ for diamond-Si (0.13 eV) in the same regime.

Notably, even though $|\bar{t}_{ij\mathbf{R}}|$ for antibonding Wannier functions are nearly zero above hopping distance of 9 Å, it does not increase monotonically below 9 Å as the hopping distance decreases. The distribution of $\bar{t}_{ij\mathbf{R}}$ (Fig. 7) is more dispersive than that of $t_{ij\mathbf{R}}$ (Fig. 6). This is likely related to the fact that the antibonding Wannier functions [Fig. 2(b)] have more nodes than the bonding Wannier functions [Fig. 2(a)]. They are also more diffuse than the bonding Wannier functions. In addition, antibonding Wannier functions hybridize with the continuum, making them somewhat sensitive to the choice of the frozen window used in the Wannier disentanglement [43] procedure. [For consistency, we have chosen the frozen windows for both diamond-Si and Si$_{20}$ to span the same energy range, from the conduction band minimum (CBM) to 3.5 eV above the CBM of diamond-Si.]

Hopping integrals between antibonding Wannier states of Si$_{20}$ are distributed over a wider energy range than diamond-Si. We expect the larger hopping integrals between the empty Wannier functions of Si$_{20}$ to increase the bandwidth of the

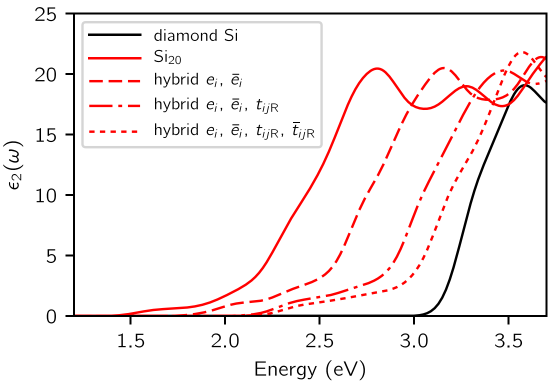

FIG. 8. Optical absorption spectra of diamond-Si (black), Si_{20} (solid red), and the three hybrid model systems (dashed, dotted-and-dashed and dotted red). These absorption curves have all been scissors-shifted to higher energy by 0.6 eV, based on the results of our *GW*-BSE calculation.

conduction bands and lower its conduction band edge. This will be further discussed in Sec. III E.

D. Position integral $\mathbf{r}_{ij\mathbf{R}}$

Now we discuss the third real-space object that is required to compute optical absorption: the position operator in the real-space representation, $\mathbf{r}_{ij\mathbf{R}}$, between a bonding Wannier function and an antibonding Wannier function. [The matrix elements between two bonding or two antibonding Wannier functions do not enter Eq. (1).]

For diamond-Si, $|\mathbf{r}_{ij\mathbf{R}}|^2$ is the largest when i and j are both centered on the same bond, as can be expected. Its value is 0.59 $\mathring{A}^2$ and it is seven times larger than its value when i and j are separately centered on two nearest-neighboring bonds (0.09 $\mathring{A}^2$). For Si_{20}, $|\mathbf{r}_{ij\mathbf{R}}|^2$ are also the largest when i and j are both centered on the same bond. Their values for the four types of Si_{20} bonds are nearly the same, averaging at $0.53 \pm 0.02\ \mathring{A}^2$. (The next largest value is only 0.15 $\mathring{A}^2$.)

Here two observations can be made. First, we see that in the real-space representation, $|\mathbf{r}_{ij\mathbf{R}}|^2$, like the Hamiltonian, is highly localized. Second, the largest $|\mathbf{r}_{ij\mathbf{R}}|^2$ for Si_{20} and diamond-Si have nearly the same numerical value. This is likely because the Wannier functions of Si_{20} have similar real-space character as those of diamond-Si.

E. Relating e_i and $t_{ij\mathbf{R}}$ to the optical absorption

Now we will relate the magnitudes of e_i and $t_{ij\mathbf{R}}$ to the optical absorptions in diamond-Si and Si_{20}. For this purpose, we will additionally compute the optical absorption spectra of three other model systems, which are hybrids of diamond-Si and Si_{20}. These hybrid systems have the same Hamiltonian as Si_{20}, except for some e_i, $\bar{e}_i$, $t_{ij\mathbf{R}}$, and $\bar{t}_{ij\mathbf{R}}$ which are modified to resemble those of diamond-Si. Figure 8 shows the calculated optical spectra of diamond-Si (in solid black), Si_{20} (in solid red), and the hybrid systems (in dashed, dotted-and-dashed, and dotted red).

The dashed red curve in Fig. 8 shows the calculated optical absorption spectrum of the first hybrid system, where all on-site energies e_i and $\bar{e}_i$ of Si_{20} are made to be equal to that of diamond-Si.

The dotted-and-dashed curve in Fig. 8 represents the second hybrid system where, on top of the modifications made for the first hybrid system, hopping integrals $t_{ij\mathbf{R}}$ between bonding Wannier functions are modified as well. This modification is done in the following way. First, we identify the nearest-neighbor hopping integrals between the bonding Wannier functions of Si_{20} that are larger in magnitude than that of diamond-Si (their values are -1.93, -1.45, -1.30, and -1.29 eV). Second, we modify these hopping integrals so that they are equal to that of diamond-Si (-1.23 eV).

Finally, the dotted red curve in Fig. 8 shows the optical absorption spectrum of the third hybrid system which, in addition to the modifications made for the first and second hybrid systems, has modified hopping integrals between the antibonding Wannier functions $\bar{t}_{ij\mathbf{R}}$. Here we follow the same logic as is used for hopping integrals between the bonding Wannier functions. We first identify the hopping integrals between the antibonding Wannier functions of Si_{20} in the nearest-neighbor regime that are larger in magnitude than that of diamond-Si (their magnitudes are 0.18, 0.20, 0.23, 0.32, 0.34, and 0.40 eV). Next, we modify their magnitudes so that they are the same as that of diamond-Si (0.13 eV).

As can be seen from Fig. 8, modifying only e_i and $\bar{e}_i$ shifts the leading edge of the absorption spectrum of Si_{20} to a higher energy by about 0.30 eV. This is about 33% of its difference with diamond-Si. Modifying e_i, $\bar{e}_i$, and $t_{ij\mathbf{R}}$ further shifts the leading edge of the absorption spectrum by another 0.30 eV. When e_i, $\bar{e}_i$, $t_{ij\mathbf{R}}$, and $\bar{t}_{ij\mathbf{R}}$ are all modified, the edge of the absorption spectrum is shifted by a total of 0.75 eV from the original calculated spectrum, accounting for approximately 83% of its difference with diamond-Si.

This behavior can be understood by considering a simple tight-binding model of a periodic one-dimensional monoatomic chain. The band structure of such a model is given by $e + 2t\cos(ka)$ where e is the on-site energy, t is the hopping integral between the nearest-neighboring orbitals, and a is the distance between atoms. Therefore, the on-site energy e can be thought of as the average energy of the band while the hopping integral t determines its bandwidth. This means that the smaller $\bar{e}_i - e_i$ and larger $t_{ij\mathbf{R}}$ and $\bar{t}_{ij\mathbf{R}}$ of Si_{20} will reduce the average band gap.

The modifications that are made to the hybrid systems do not account for the remaining 17% and an absorption tail at low energy. We attribute this to the following two effects. First, we only modified some of the larger hopping integrals in our calculations of the hybrid models. Second, even though we modified the hopping integrals in our calculations, we have always kept the crystal structure of Si_{20} the same. Therefore, relative phases of the Bloch states between neighboring silicon-bond sites in Si_{20} will be different from those in diamond-Si. In other words, even if the hopping integrals were somehow made exactly the same in the two structures, their optical absorption edges may still not be the same because of this effect. Nevertheless, the total influence of these two effects on the improved optical absorption of Si_{20} is rather small (17%) and the majority of the difference can be attributed to the differences in the on-site energies and hopping integrals.

F. SC5 and Si_{24} silicon phases

To demonstrate the generality of our approach, we consider now two other phases of silicon that also absorb light (without phonon-assisted transitions) at photon energy lower than diamond-Si. The first phase can be described as a Si superlattice composed of alternating stacks of bulklike Si layers intercalated by Seiwatz chains [31]. Each stack is made of five Si(111) layers of hexagonal diamond-Si. The Seiwatz chains are arranged in a configuration that results in a simple monoclinic Bravais lattice. We refer to this phase as SC5. The second phase is a low-density Si_{24} structure with an open silicon framework [23]. Unlike Si_{20} that we have discussed in detail earlier, none of these two phases have Si-Si bonds in a triangular arrangement.

Repeating the earlier analysis for SC5, we find that all of its bonds have $\bar{e}_i - e_i$ smaller than that in diamond-Si. In SC5, they range from 9.09 to 9.61 eV. If we change the on-site energies of SC5 to match that of diamond-Si, we find that the optical spectrum shifts to a higher energy, more closely resembling that of diamond-Si. This change in the on-site energies accounts for roughly 70% of the change in the optical absorption. Furthermore, if we also change the hopping integrals of SC5 to match those of diamond-Si, we find another 20% change in the optical absorption. Therefore, the improved calculated optical absorption edge of SC5 is mostly due to changes in the on-site energies, not hopping integrals. This is in contrast to Si_{20}, where the dominant effect comes from the hopping integrals.

Switching to Si_{24}, our calculation shows that most of its on-site energy differences ($\bar{e}_i - e_i$) are larger than that of diamond-Si. Out of the 24 bonds in the primitive unit cell of Si_{24} (the primitive unit cell of Si_{24} only has 12 atoms), 18 bonds have larger on-site energy differences than that of diamond-Si while only six bonds have smaller on-site energy differences. The range of $\bar{e}_i - e_i$ in Si_{24} spans from 9.18 to 10.69 eV. We attribute this to Si_{24}'s open silicon framework and its low density ($2.17\,\mathrm{g/cm^3}$) [23] as compared to that of diamond-Si (see Sec. III A). If we modify the on-site energies of Si_{24} so that they are equal to that of diamond-Si, we find that the onset of optical absorption shifts to a lower energy. If we also modify the hopping integrals, the optical absorption spectrum now shifts to higher energy and more closely matches that of diamond-Si. Therefore, we conclude that in the case of Si_{24}, the effect of the on-site energies on the optical absorption is opposite to that of the hopping integrals.

IV. CONCLUSION

The different structure of Si_{20}, relative to diamond-Si, leads to smaller on-site energy differences and larger hopping integrals between some of its Wannier functions. We have identified that most of these differences are due to the strained bonds forming triangles (i.e., type-a bonds) in Si_{20}. Different on-site energies and large hopping integrals are responsible for approximately 83% of the improved optical absorption in Si_{20} for photovoltaic applications relative to diamond-Si. The remaining difference is attributed to contributions from the smaller hopping integrals and the effect of the crystal structure on the relative phase of the electron wave functions.

Introducing strain to the bonds in the crystal structure turns out to be important when looking for crystal phases of silicon that have band gaps smaller than diamond-Si. However, just as strain may reduce the band gap of diamond-Si, it also reduces the stability of the crystal structure. It is possible that a large band gap reduction may require a strain that is too large for the crystal structure to be thermodynamically stable. Hence, in the search for a practically viable silicon crystal phase that has a band gap smaller than that of diamond-Si, it is a balance between reducing the band gap and increasing the strain in the crystal structure.

ACKNOWLEDGMENTS

This work was supported by National Science Foundation Grant No. DMR-1508412 which provided for the DFT calculations and the Wannier functions analysis, and by the Theory of Materials Program at the Lawrence Berkeley National Lab funded by the Director, Office of Science and Office of Basic Energy Sciences, Materials Sciences and Engineering Division, U.S. Department of Energy under Contract No. DE-AC02-05CH11231 which provided for the *GW*-BSE calculations. Computational resources have been provided by the DOE at Lawrence Berkeley National Laboratory's NERSC facility. C.S.O. acknowledges support from the Singapore National Research Foundation (Clean Energy) PhD Scholarship.

---

[1] *ASTM G173-03(2012) Standard Tables for Reference Solar Spectral Irradiances: Direct Normal and Hemispherical on 37° Tilted Surface* (ASTM International, West Conshohocken, PA, 2012).

[2] W. Shockley and H. J. Queisser, J. Appl. Phys. **32**, 510 (1961).

[3] S. Rühle, Solar Energy **130**, 139 (2016).

[4] H. J. Queisser, Mater. Sci. Eng. B **159-160**, 322 (2009).

[5] J. Noffsinger, E. Kioupakis, C. G. Van de Walle, S. G. Louie, and M. L. Cohen, Phys. Rev. Lett. **108**, 167402 (2012).

[6] G. G. Macfarlane, T. P. McLean, J. E. Quarrington, and V. Roberts, Phys. Rev. **111**, 1245 (1958).

[7] J. C. Jamieson, Science **139**, 762 (1963).

[8] M. I. McMahon, R. J. Nelmes, N. G. Wright, and D. R. Allan, Phys. Rev. B **50**, 739 (1994).

[9] H. Olijnyk, S. Sikka, and W. Holzapfel, Phys. Lett. A **103**, 137 (1984).

[10] J. Hu and I. Spain, Solid State Commun. **51**, 263 (1984).

[11] K. J. Chang and M. L. Cohen, Phys. Rev. B **30**, 5376 (1984).

[12] K. J. Chang, M. M. Dacorogna, M. L. Cohen, J. M. Mignot, G. Chouteau, and G. Martinez, Phys. Rev. Lett. **54**, 2375 (1985).

[13] M. Hanfland, U. Schwarz, K. Syassen, and K. Takemura, Phys. Rev. Lett. **82**, 1197 (1999).

[14] R. O. Piltz, J. R. Maclean, S. J. Clark, G. J. Ackland, P. D. Hatton, and J. Crain, Phys. Rev. B **52**, 4072 (1995).

[15] S. Minomura and H. Drickamer, J. Phys. Chem. Solids **23**, 451 (1962).

[16] J. Kasper and S. Richards, Acta Crystallogr. **17**, 752 (1964).

[17] R. H. Wentorf Jr. and J. S. Kasper, Science **139**, 338 (1963).

[18] B. D. Malone, J. D. Sau, and M. L. Cohen, Phys. Rev. B **78**, 035210 (2008).

[19] Y.-X. Zhao, F. Buehler, J. R. Sites, and I. L. Spain, Solid State Commun. **59**, 679 (1986).

[20] B. D. Malone, J. D. Sau, and M. L. Cohen, Phys. Rev. B **78**, 161202 (2008).

[21] B. D. Malone, S. G. Louie, and M. L. Cohen, Phys. Rev. B **81**, 115201 (2010).

[22] M. L. Cohen and B. D. Malone, J. Appl. Phys. **109**, 102402 (2011).

[23] D. Y. Kim, S. Stefanoski, O. O. Kurakevych, and T. A. Strobel, Nat. Mater. **14**, 169 (2014).

[24] Y. Wang, J. Lv, L. Zhu, and Y. Ma, Phys. Rev. B **82**, 094116 (2010).

[25] T. F. T. Cerqueira, R. Sarmiento-Pérez, M. Amsler, F. Nogueira, S. Botti, and M. A. L. Marques, J. Chem. Theory Comput. **11**, 3955 (2015).

[26] C. J. Pickard and R. J. Needs, Phys. Rev. Lett. **97**, 045504 (2006).

[27] I.-H. Lee, Y. J. Oh, S. Kim, J. Lee, and K. Chang, Comput. Phys. Commun. **203**, 110 (2016).

[28] S. Botti, J. A. Flores-Livas, M. Amsler, S. Goedecker, and M. A. L. Marques, Phys. Rev. B **86**, 121204 (2012).

[29] Q. Wang, B. Xu, J. Sun, H. Liu, Z. Zhao, D. Yu, C. Fan, and J. He, J. Am. Chem. Soc. **136**, 9826 (2014).

[30] I.-H. Lee, J. Lee, Y. J. Oh, S. Kim, and K. J. Chang, Phys. Rev. B **90**, 115209 (2014).

[31] Y. J. Oh, I.-H. Lee, S. Kim, J. Lee, and K. J. Chang, Sci. Rep. **5**, 18086 (2015).

[32] R. Seiwatz, Surf. Sci. **2**, 473 (1964).

[33] H. J. Xiang, B. Huang, E. Kan, S.-H. Wei, and X. G. Gong, Phys. Rev. Lett. **110**, 118702 (2013).

[34] Y. Guo, Q. Wang, Y. Kawazoe, and P. Jena, Sci. Rep. **5**, 14342 (2015).

[35] M. Amsler, J. A. Flores-Livas, S. Botti, M. A. L. Marques, and S. Goedecker, Phys. Rev. Lett. **112**, 199801 (2014).

[36] H. J. Xiang, B. Huang, E. Kan, S.-H. Wei, and X. G. Gong, Phys. Rev. Lett. **112**, 199802 (2014).

[37] P. Giannozzi *et al.*, J. Phys.: Condens. Matter **21**, 395502 (2009).

[38] M. S. Hybertsen and S. G. Louie, Phys. Rev. B **34**, 5390 (1986).

[39] C. S. Ong, B. A. Barker, and S. G. Louie (unpublished).

[40] M. Rohlfing and S. G. Louie, Phys. Rev. B **62**, 4927 (2000).

[41] N. Marzari and D. Vanderbilt, Phys. Rev. B **56**, 12847 (1997).

[42] C. Brouder, G. Panati, M. Calandra, C. Mourougane, and N. Marzari, Phys. Rev. Lett. **98**, 046402 (2007).

[43] I. Souza, N. Marzari, and D. Vanderbilt, Phys. Rev. B **65**, 035109 (2001).